

$(d - 2)$ -dimensional edge states of rotation symmetry protected topological states

Zhida Song,^{1,2} Zhong Fang,^{1,3} and Chen Fang^{1,*}

¹*Beijing National Laboratory for Condensed Matter Physics and Institute of Physics,
Chinese Academy of Sciences, Beijing 100190, China*

²*University of Chinese Academy of Sciences, Beijing 100049, China*

³*Collaborative Innovation Center of Quantum Matter, Beijing, 100084, China*

We study fourfold rotation invariant gapped topological systems with time-reversal symmetry in two and three dimensions ($d = 2, 3$). We show that in both cases nontrivial topology is manifested by the presence of the $(d - 2)$ -dimensional edge states, existing at a point in 2D or along a line in 3D. For fermion systems without interaction, the bulk topological invariants are given in terms of the Wannier centers of filled bands, and can be readily calculated using a Fu-Kane-like formula when inversion symmetry is also present. The theory is extended to strongly interacting systems through explicit construction of microscopic models having robust $(d - 2)$ -dimensional edge states.

I. INTRODUCTION

A symmetry protected topological state (SPT) is a gapped quantum state that cannot be continuously deformed into a product state of local orbitals without symmetry breaking^{1,2}. SPT is known to have gapless boundary states in one lower dimension³, i. e., the $(d - 1)$ -dimensional edge, such as the spin-1/2 excitations at the end of a Haldane chain⁴ or the Dirac surface states at the surface of a topological insulator^{5,6}. The gapless states are protected by the symmetries on the $(d - 1)$ -dimensional edge, and when the symmetry is a spatial symmetry, they only appear on the boundary that is invariant under the symmetry operation⁷⁻¹⁰.

Very recently, the possibility of having gapped $d - 1$ -dimensional edge but gapless $d - 2$ -dimensional edge has been discussed^{11,12}. In Ref. [11], it was shown that in a 2D spinless single particle (i.e., no spin-orbit coupling) system that has anti-commuting mirror planes, all four side edges can be gapped without symmetry breaking on an open square, but there are four modes localized at the four corners (0D edge) protected by mirror symmetries. Here we first extend the theory of 0D edge states to spin-1/2 fermion systems without mirror symmetries but with fourfold rotation symmetry and time-reversal symmetry. We point out that the presence of 0D-edge states can be understood as the result of a mismatch between the locations of the centers of the Wannier states and those of atoms. Then we generalize the theory to 3D, and define a new topological invariant by classifying the ‘spectral flow’ of the Wannier centers between the $k_z = 0$ - and the $k_z = \pi$ -slices in the Brillouin zone. When this invariant is nontrivial, there are four helical edge modes on the otherwise gapped side surfaces of the 3D system. We further show that when space inversion is also present, there is a Fu-Kane-like formula¹³ relating this invariant to certain combinations of rotation and inversion eigenvalues of the filled bands at high-symmetry crystal momenta. Finally, we generalize the theory to strongly interacting systems, by constructing microscopic models of boson and fermion SPT states that have $(d - 2)$ -dimensional edge states for $d = 2, 3$ using coupled wires construction. We remark

that these edge states, protected by C_4 and some local symmetry such as time-reversal, are not pinned to the corners or hinges of the system, and can even appear in geometries having smooth side surfaces.

II. MISMATCH BETWEEN THE ATOM SITES AND THE WANNIER CENTERS

Wannier functions for the filled bands can be constructed for all 2D gapped insulator that have zero Chern number¹⁴. When symmetries are involved (time-reversal and/or spatial), the set of Wannier functions may or may not form a representation of the symmetry group¹⁵. If they do, then we call these Wannier functions ‘symmetric’. If a set of symmetric Wannier functions cannot be found for all filled bands, we know that the system cannot be adiabatically deformed into an atomic insulator: this is considered a generalized definition of topologically nontrivial insulators^{16,17}, since atomic orbitals automatically form a set of symmetric wavefunctions. Atomic insulators are usually considered trivial. Nevertheless, we realize that even they can also be somewhat nontrivial if there is a mismatch between the Wannier centers and the atomic positions, as shown in Fig. 1(a). A Wannier center (WC) can be understood as the middle of the Wannier function (but see appendix A for a rigorous definition), and if the Wannier functions are symmetric, their centers are also symmetric. When the mismatch happens, it means that while the insulator can be deformed into some atomic insulator, it would not be made by the atoms forming the lattice. The presence of 0D edge states of the system put on an open disk is the manifestation of the ‘mismatch’.

To be specific, let us consider a square lattice model

$$H = (1 - \cos k_x - \cos k_y) \tau_0 \sigma_z s_0 + \sin k_x \tau_0 \sigma_x s_x + \sin k_y \tau_0 \sigma_x s_y + \Delta (\cos k_x - \cos k_y) \tau_y \sigma_y s_0, \quad (1)$$

in which all the atomic orbitals are put on the lattice sites. Here τ_i, σ_i ($i = 0, x, y, z$) are Pauli matrices representing the orbital degrees of freedom, and s_i ($i = 0, x, y, z$) representing the spin. This model can be

thought as two copies of 2D topological insulator plus a mixing term with Δ as coefficient; and it has time-reversal symmetry $T = -is_y K$ and a rotation symmetry $C_4 = \tau_z e^{-i\pi s_z/4}$. The system put on a torus is fully gapped because the four terms in Eq. (1) anti-commute with each other and their coefficients do not vanish at the same time.

As shown in appendix B 3, whatever value Δ takes, the insulator is equivalent to an atomic one, and its WC are located at the plaquette centers. We have explicitly constructed a set of symmetric Wannier functions and prove that, protected by the time-reversal and C_4 symmetries, the Wannier centers stay invariant under any gauge transformation that keeps the Wannier functions symmetric. This model hence realizes the mismatch between the WCs at plaquette centers and the atomic positions at sites.

Now we cut along the dotted lines in Fig. 1(a) and turn the 2D torus into an open square. Since this cut preserves C_4 symmetries, the states centered at the plaquette center will be equally divided into the four quarters, so that each quarter carries one extra electron on top of some even integer filling. Due to T , this means that a pair (Kramers' pair) of zero modes are located near each of the four corners of the square. One may observe that in the absence of particle-hole symmetry (which is an accidental symmetry of the model), the modes can be moved away from zero and pushed into the bulk states, but we argue that even when this happens, the corners are still nontrivial in the following sense. The total eight modes (two near each corner) come from both the conduction and the valence bands, each having $(N_{band} - \nu)L^2 - 4$ and $\nu L^2 - 4$ electrons respectively, where $N_{band} \in \text{even}$ and $\nu \in \text{even}$ are the total number of bands and the filling number respectively, and L the length of the square (Fig. 1(b)). No matter where the Fermi energy is, a gapped ground state must have $4 \bmod 8$ electrons on an even-by-even lattice, so that each corner has exactly one (or minus one) extra electron on top of the filling of the bulk. This is in sharp contrast with the systems having trivial corner states, whose energy levels are plotted in Fig. 1(c). In that case, the in-gap states can be pushed into the conduction bulk and there is no extra charge at each corner. In Fig. 1(d)-(e), we plot the charge density at $\mu = \mu_1$ in real space, and plot the extra electric charge within a small area near the corner as a function of radius in the Slater-product many-body ground state.

III. 1D HELICAL STATE AND \mathbb{Z}_2 WANNIER CENTER FLOW

A natural generalization of the 0D state in 2D is the 1D edge state in 3D, where both the 3D bulk and 2D side surfaces are insulating, as shown in Fig. 2(c). Our construction of this state is also based on the WC picture. Assume the 3D system has T and C_4 symmetries, so we can take a C_4 invariant tetragonal cell and transform the

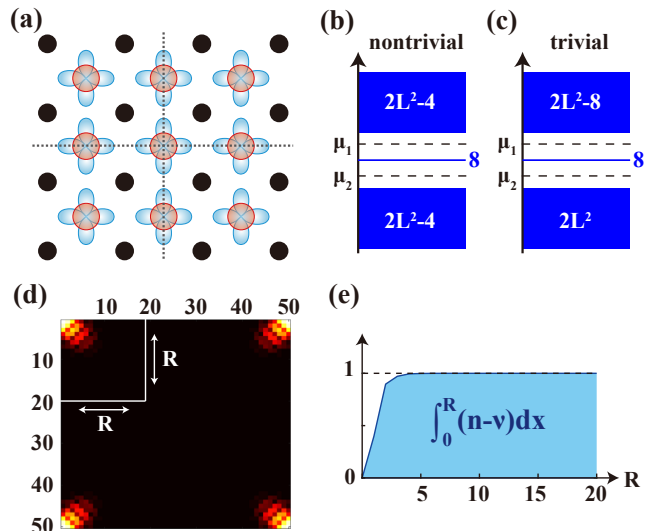


FIG. 1. Nontrivial 0D edge modes of 2D fermion. In (a) we sketch the mismatch between the atom sites and the WCs, where the atom sites are represented by the block circles and the WFs are represented by the colored orbitals. In (b) and (c), level counting for systems with nontrivial and with trivial 0D edge state are shown, respectively. In (d) the numerical calculated density profile of the 2D model with a finite size of 50×50 is plotted, where the Fermi level is set at μ_1 . The four bright regions in (d) show the additional charges located at the corners. To count the number of additional charges around a corner, we plot the integral of the density deviation from the filling ($\nu = 4$) in (e).

Hamiltonian along the z -direction to momentum space. Each slice with fixed k_z can be thought as a 2D system, wherein the $k_z = 0, \pi$ -slices are time-reversal and C_4 invariant while the others are only C_4 invariant. Consider an insulator that has four filled bands, or four WCs for each k_z -slice. Due to C_4 , the four WCs are related to each other by fourfold rotations; and due to T , at $k_z = 0$ or $k_z = \pi$, two WCs that form a Kramers' pair must coincide. Therefore, at $k_z = 0$ and $k_z = \pi$, there are only three possible configurations for the four WC: all four at $1a$, all four at $1b$ and two at each $2c$ Wyckoff positions. If the configurations at $k_z = 0$ and at $k_z = \pi$ are different, the evolution of the WC between the two slices forms a ' \mathbb{Z}_2 -flow', a robust topological structure revealing that the 3D insulator is not an atomic one. Out of several different combinations of the configurations at $k_z = 0$ and $k_z = \pi$, there are two topologically distinct \mathbb{Z}_2 -flows, where the four WCs flow from $1b$ to $1a$ and from $1b$ to $2c$ [solid yellow and dashed green lines in Fig. 2(a)], respectively. The latter \mathbb{Z}_2 -flow can be shown equivalent to a weak topological index (appendix C 1), and we from now on focus on the first \mathbb{Z}_2 -flow from $1b$ to $1a$. Whether this flow is present or not gives us a new \mathbb{Z}_2 -invariant, and its edge manifestation is the existence of 1D helical edge modes on the side surface of a bulk sample. (For more rigorous definition and classification of the WC flow for

arbitrary number of filled bands, see appendix C 1.)

To see this bulk-edge correspondence, we cut the bulk along both x and y directions, keeping the periodic boundary condition along z . From top-down perspective, a corner of the sample takes the shape of the dotted lines shown in Fig. 2(a). One can see that at the corner, the boundary cuts through exactly one (or three) line in the WC flow, corresponding to one helical mode along the hinge between the two open surfaces. To make the picture more concrete, we consider the following 3D model, which is a simple extension of the 2D model in Eq. (1).

$$H = \left(2 - \sum_i \cos k_i\right) \tau_0 \sigma_z s_0 + \sum_i \sin k_i \tau_0 \sigma_x s_i + \Delta (\cos k_x - \cos k_y) \tau_y \sigma_y s_0 \quad (2)$$

The $k_z = 0$ -slice is equivalent with the 2D model in Eq. (1), thus having four charges locating at the plaquette center. The $k_z = \pi$ -slice is, however, a 2D atomic insulator with four charges locating at the lattice site. The mismatch between the WCs at $k_z = 0$ - and $k_z = \pi$ -slices means that the \mathbb{Z}_2 -flow exists. To confirm the \mathbb{Z}_2 -flow, we also choose a smooth gauge for all the k_z slices from $k_z = 0$ to $k_z = \pi$ and plot the WC flow explicitly, which indeed gives the \mathbb{Z}_2 -flow, shown in appendix C 2. The 1D helical state is also confirmed by a numerical calculation of the band structure of a finite tetragonal cylinder, as plotted in Fig. 2(b). For this particular model, the helical edge states can be viewed from another perspective. The edge between the two open surface can be considered as the domain wall between them. On each surface there is a mass gap, and the rotation symmetry in this model enforces the two masses to be opposite, so that at the domain wall there is a helical mode¹⁰ [see Fig. 2(c) for a schematic and see appendix D for more details].

IV. SYMMETRY INDICATORS FOR THE \mathbb{Z}_2 -INVARIANT

To see if a given insulator has 1D helical edge modes on the side surface, one needs to calculate the evolution of the WCs as a function of k_z , which in turn requires finding symmetric, smooth and periodic Bloch wave functions for all bands at each k_z -slice as is done for the our model Hamiltonian. This is practically impossible in real materials. Now we show that in the presence of additional inversion symmetry, this \mathbb{Z}_2 -invariant can be determined by the rotation and inversion eigenvalues at all high-symmetry momenta, simplifying the diagnosis. We call this method a ‘‘Fu-Kane-like formula’’, likening it to the Fu-Kane formula for time-reversal topological insulators¹³, where inversion is not required to protect the nontrivial topology, but when present greatly simplifies the calculation.

This formula is derived based on the new theory of symmetry indicators^{16,17}: given any insulator, a full set

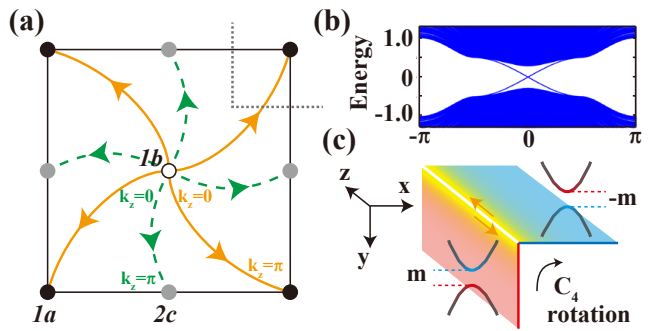


FIG. 2. Nontrivial 1D helical modes of 3D insulator. In (a) we plot the two generators of nontrivial \mathbb{Z}_2 -flows from the $k_z = 0$ -slice to the $k_z = \pi$ -slice, where the lattice site (1a), the plaquette center (1b), and the edge midpoint (2c) are represented by black planchet, hollow circle, and grey planchet, respectively. In (b) the numerically calculated helical modes of our 3D model on a tetragonal cylinder geometry is plotted. The length along x and y directions is 50. In (c) we sketch the domain wall between surfaces of opposite masses, enforced by the C_4 rotation symmetry.

of eigenvalues of the space group symmetry operators for filled bands at all high-symmetry points generates a series of indicators. They tell us if this set is consistent with any atomic insulator, and if yes, the theory further gives where the atomic orbitals are located. Our goal is to find such an indicator that is equivalent to the \mathbb{Z}_2 -invariant for the WC flow. Following the WC flow picture, we require: (i) at $k_z = 0$ and $k_z = \pi$, the eigenvalues of C_4 , $C_2 = C_4^2$ and P are consistent with atomic insulators; (ii) there is no surface state on the side surfaces; and (iii) comparing the two slices at $k_z = 0$ and $k_z = \pi$, the numbers of atomic orbitals at 1a and at 1b change by ± 4 and ∓ 4 , respectively. For a concrete example, let us consider space group $P4/m$, whose indicators form a group $\mathbb{Z}_2 \times \mathbb{Z}_4 \times \mathbb{Z}_8$ ¹⁶, so that insulator according to its C_4 and P eigenvalues can be denoted by (mnl) ($m = 0, 1$, $n = 0, 1, 2, 3$, $l = 0, 1, \dots, 7$), and an insulator with a nonzero indicator cannot be adiabatically deformed into an atomic insulator. Using the three criteria above, we find that the \mathbb{Z}_2 -flow is nontrivial only if $(mnl) = (004)$. Similar calculation can be done for all space groups having both C_4 and P . (See appendix E for the results, and find a MATLAB script therein for automated diagnosis for materials in these space groups.)

V. EXTENSION TO STRONGLY INTERACTING SPT

In the above we have established the theory of $(d-2)$ -dimensional edge modes for free fermions through the WC picture. Since WC is a single particle object, the same picture does not apply for strongly interacting bosons or fermions. Here we rebuild a 3D free fermion model with robust 1D helical edge modes using cou-

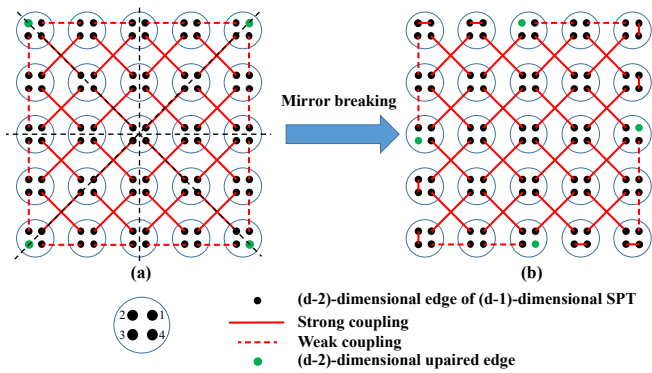


FIG. 3. Coupled wires construction for a 3D SPT with robust 1D edge modes. Each filled circle is a wire from topdown, and each open circle including four elementary wires is a ‘physical’ wire that can be realized in 1D lattice models. The breaking of mirror symmetry in (a) causes the edge modes to move to the positions in (b).

pled wires construction^{18–20}, a method that can be easily extended to strongly interacting SPT. These SPT can either be bosonic²¹ or fermionic, and are in general protected by spatial symmetry²² plus some internal symmetry²³.

Consider an arrangement of 1D wires shown in top-down view in Fig. 3(a), each of which represents a helical mode. Due to the fermion doubling theorem, each wire alone cannot be physically realized in 1D, but an even number of these wires can be realized as a 1D wire fine tuned to a critical point. In our model, four wires make a physical, critical 1D wire. For concreteness we assume that under C_4 -rotation the four wires inside cyclically permute. Then we couple the wires in the following way: the four wires, in topdown view, which share a plaquette are coupled diagonally, i.e., 1 coupled to 3 and 2 to 4. For a 3D torus these couplings (solid red lines) make the coupled wire system an insulator. For a cylinder geometry open in x and y directions, however, there are ‘dangling helical wires’ on the side surfaces, which can again be gapped by turning on a dimerizing coupling (dotted lines). But one soon discovers that, as long as C_4 is preserved, there are always four unpaired wires on the side surface (represented by green dots), which are in fact the same 1D helical edge mode protected by C_4 and T studied above.

This construction can be easily extended to strongly interacting SPT. One simply replaces each helical wire with a $(d-2)$ -dimensional edge of a $(d-1)$ -dimensional SPT protected by some local symmetry. For example, each ‘wire’ can be a 0D spin-1/2, which is the edge of a 1D Haldane chain protected by $SO(3)$ symmetry. In that case, the resultant construction in Fig. 3(a) is nothing but an AKLT-like state^{24,25} formed by $S=2$ spins, but unlike previously considered AKLT states in 2D, it has gapped 1D edge but four 0D gapless spin-1/2 excitations localized at the four corners in an open square. We can also replace each wire by the edge of a Levin-Gu state²⁶,

protected by a \mathbb{Z}_2 local symmetry, then the construction in Fig. 3(a) is a 3D bosonic SPT with 1D gapless modes at four corners. Notice that in these boson examples, time-reversal symmetry is not necessary. Similar construction can be used to obtain SPT states protected by both the local symmetries (being T , $SO(3)$ or \mathbb{Z}_2) and C_4 -rotation symmetry.

VI. DISCUSSION

It is important to note that, while in examples studied so far, the $(d-2)$ -dimensional edge modes sit at the corners or hinges in the disk or cylinder geometry, it is not always the case. In the model shown in Fig. 3(a), the edge modes are pinned to the corners by the mirror symmetries (dotted lines), and breaking these mirror planes in the bulk or on the surface causes the edge modes to move away. In the example shown in Fig. 3(b), we break the mirror symmetry of the construction on the surface, so that the dangling wires move from the corners to some generic points on the side. As long as C_4 is present, the $(d-2)$ -dimensional edge modes are stable, yet not pinned to corners or hinges in the absence of mirror symmetries. In fact, they still appear even if the whole side surface is smooth without hinges at all. We also emphasize that while these edge modes are protected by C_4 -rotation symmetry, breaking the symmetry perturbatively in the bulk or on the boundary does not in general gap out the modes, because time-reversal alone is sufficient to protect 1D helical edge modes. The only way of gapping the modes is to annihilate them in pairs, and this means large C_4 -breaking either in the bulk or on the boundary. Similar discussions may be extended to systems with twofold, threefold, sixfold rotations.

Experimentally, the four helical edge modes of a 3D electronic insulator contribute a quantized conductance of $4e^2/h$ that may be measured in electric transport⁶. Also the $(d-2)$ -dimensional edge modes may be detected by local probes such as scanning tunneling microscopy, either on a bulk sample or at the step edge of a thin film.

ACKNOWLEDGMENTS

C. F. thanks Xi Dai, Yuan-Ming Lu, Meng Cheng, Yang Qi and B. Andrei Bernevig for helpful discussion. The work was supported by the National Key Research and Development Program of China under grant No. 2016YFA0302400, by NSFC under grant No. 11674370.

Appendix A: A brief review of Wannier functions

Wannier functions (WFs) are defined as the Fourier transformations of Bloch wave functions, with a gauge

freedom

$$|w_{\alpha\mathbf{R}}\rangle = \frac{1}{\sqrt{\mathcal{N}}} \sum_{\mathbf{k}\alpha} e^{-i\mathbf{k}\cdot\mathbf{R}} |\phi_{\alpha\mathbf{k}}\rangle \quad (\text{A1})$$

$$|\phi_{\alpha\mathbf{k}}\rangle = \sum_n U_{n\alpha}(\mathbf{k}) |\psi_{n\mathbf{k}}\rangle \quad (\text{A2})$$

Here $|\psi_{n\mathbf{k}}\rangle$ is the n -th Bloch state at \mathbf{k} , \mathbf{R} is a lattice vector in real space, \mathcal{N} is the number of cells, α is the wannier index, and $U(\mathbf{k})$ can be an arbitrary unitary matrix. Generally speaking, as long as $|\phi_{\alpha\mathbf{k}}\rangle$ takes a smooth gauge in the whole Brillouin zone, the corresponding WF $|w_{\alpha\mathbf{R}}\rangle$ will be well localized around the lattice \mathbf{R} .

The WC is defined as the position expectation on the WF. It can be calculated from the Berry connection in momentum space

$$\langle w_{\alpha\mathbf{R}} | \hat{\mathbf{x}} | w_{\alpha\mathbf{R}} \rangle = \int \frac{d^d\mathbf{k}}{(2\pi)^d} \mathcal{A}_\alpha(\mathbf{k}) + \mathbf{R} \quad (\text{A3})$$

where the Berry connection is defined as

$$\mathcal{A}_\alpha(\mathbf{k}) = i \sum_{mn} \langle U_{m\alpha} u_m | \partial_{\mathbf{k}} | U_{n\alpha} u_n \rangle \quad (\text{A4})$$

and $u_n(\mathbf{k})$ is the periodic part of the Bloch wavefunction $|\psi_{n\mathbf{k}}\rangle$. In general, WCs are gauge dependent, i.e. they depend on the choice of the gauge $U_{n\alpha}(\mathbf{k})$. An exception is the 1D insulating system where the 1D WCs can be thought as the spectrum of the wilson loop along the 1D Brillouin zone and thus are gauge invariant quantities. Such a property leads to the modern theory of polarization^{27,28} and has greatly facilitated the studies of topological insulators because the spectrum of wilson loop is believed to be isomorphic with the surface dispersion^{29,30}.

To define the symmetric WFs, let us firstly review the concept of wyckoff positions in real space. General positions in the unit cell can be classified into a few types of wyckoff positions by their site symmetry groups (SSGs). The SSG for a given site \mathbf{x}_1 can be defined as the collection of all the space group elements that leave \mathbf{x}_1 invariant (module a lattice vector), i.e.

$$G(\mathbf{x}_1) = \{g \in G | \exists \mathbf{R} \text{ s.t. } g\mathbf{x}_1 = \mathbf{x}_1 + \mathbf{R}\} \quad (\text{A5})$$

Here $g\mathbf{x} = p_g\mathbf{x}_1 + \mathbf{t}_g$ with p_g the point group operation of g and \mathbf{t}_g the translational operation of g . The equivalent positions of \mathbf{x}_1 can be generated from a complete set of the representatives of the quotient group $G/G(\mathbf{x}_1)$

$$\mathbf{x}_\sigma = g\mathbf{x}_1 - [g\mathbf{x}_1] \quad g \in G/G(\mathbf{x}_1) \quad (\text{A6})$$

where $g_1 = e$ is the identity, and $[g\mathbf{x}_1]$ is the lattice containing $g\mathbf{x}_1$ such that \mathbf{x}_σ locates at the home cell. Hereafter, for convenience some times we will split the Wannier index α into a site index σ and an orbital index μ , indicating that the WF is the μ -th orbital locating at the

site \mathbf{x}_σ . A set of WFs is called symmetric if (i) they form representations (reps) of the SSGs of the sites they locate at

$$\forall g \in G(\mathbf{x}_\sigma) \quad g |w_{\sigma\mu\mathbf{R}}\rangle = \sum_\nu D_{\nu\mu}(g) |w_{\sigma\nu, \mathbf{R}+[g\mathbf{x}_\sigma]}\rangle \quad (\text{A7})$$

(ii) WFs at a general equivalent position of \mathbf{x}_1 can be generated from the WFs at \mathbf{x}_1 by a symmetry operation relating the two positions, and (iii) for time-reversal invariant systems, we further ask the WFs to form Kramers' pairs, i.e.

$$T |w_{\alpha\mathbf{R}}\rangle = \sum_\beta \Omega_{\beta,\alpha} |w_{\beta\mathbf{R}}\rangle \quad (\text{A8})$$

where

$$\Omega = \begin{bmatrix} 0 & -\mathbb{I} \\ \mathbb{I} & 0 \end{bmatrix} \quad (\text{A9})$$

The transformations of $|\phi_{\sigma\mu\mathbf{k}}\rangle$ under symmetry operations are completely determined by the symmetry property of WFs. For the space groups considered in our work, we have

$$\forall g \in G \quad g |\phi_{\sigma\mu\mathbf{k}}\rangle = \sum_{\sigma'\mu'} D_{\sigma'\mu',\sigma\mu}^{\mathbf{k}}(g) |\phi_{\sigma'\mu'g\mathbf{k}}\rangle \quad (\text{A10})$$

$$D_{\sigma'\mu',\sigma\mu}^{\mathbf{k}}(g) = \delta'_{\mathbf{x}_{\sigma'}, g\mathbf{x}_\sigma} e^{ig\mathbf{k}\cdot(\mathbf{x}_{\sigma'} - g\mathbf{x}_\sigma)} D_{\mu'\mu}(g) \quad (\text{A11})$$

, where $\delta'_{\mathbf{x}_{\sigma'}, g\mathbf{x}_\sigma} = 1$ if $\mathbf{x}_{\sigma'} = g\mathbf{x}_\sigma$ module a lattice, and

$$T |\phi_{\alpha\mathbf{k}}\rangle = \sum_\beta \Omega_{\beta,\alpha} |\phi_{\beta,-\mathbf{k}}\rangle \quad (\text{A12})$$

The transformation matrices $D^{\mathbf{k}}$ and Ω will be referred as the sewing matrices in the following.

Appendix B: Gauge invariant 2D Wannier centers

The discussion about the mismatch between atom sites and WCs in the text presumes the gauge invariance of the occupied 2D WCs. Otherwise, we can choose a gauge where the WCs move away from the plaquette center to negative all the arguments. Similarly, the gauge invariance of the \mathbb{Z}_2 -flow discussed in the text also needs the 2D WCs at $k_z = 0, \pi$ -slices to be gauge invariant. Here, we will set such a cornerstone by proving that in some special cases the 2D WCs indeed are gauge invariant guaranteed by the crystalline symmetry.

Since all the symmetry properties of symmetric WFs are encoded in the sewing matrices, in the proof below we follow the logic that two sets of symmetric WFs can be deformed to each other only if the sewing matrices generated from them can be transformed to each other by a smooth gauge transformation. A relevant useful

SSG	W	K	Coordinates	irreps at W	irreps at K
C_4	$1a$	Γ	$(0, 0)$	$E_{\frac{1}{2}} E_{\frac{3}{2}}$	$E_{\frac{1}{2}} E_{\frac{3}{2}}$
	$1b$	M	$(\frac{1}{2}, \frac{1}{2})$	$E_{\frac{1}{2}} E_{\frac{3}{2}}$	$E_{\frac{1}{2}} E_{\frac{3}{2}}$
C_2	$2c$	X	$(0, \frac{1}{2})$	$E_{\frac{1}{2}}$	$E_{\frac{1}{2}}$
C_1	$4d$...	(x, y)	$E_{\frac{1}{2}}$	E

TABLE I. The wyckoff positions and high-symmetry momenta in 2D space group $p4$ (with time-reversal symmetry). Due to the time-reversal symmetry, all the irreps at wyckoff positions and time-reversal invariant momenta are double degenerate. The notations of irreps follow Ref. [31].

concept is the band rep (BR), i.e. the set of reps at high-symmetry momenta, which is indeed the diagonal blocks of sewing matrices in momentum space. In some cases, the information in BR is enough to demonstrate two sets of WFs are inequivalent. Therefore, before the proof, let us figure out what BR can tell us. The smallest 2D space group containing C_4 is $p4$. As shown in table I, it has four types of wyckoff positions in real space, wherein the $1a$ and $1b$ positions are the site and plaquette center, respectively. To describe the BR we only need to count the irreps at Γ and M , because the irreps at X and general momentum are always same. After a few derivations according to Eq. (A11), we find the mappings from symmetric WFs to BRs as

$$E_{\frac{1}{2}}^{1a} \mapsto E_{\frac{1}{2}}^{\Gamma} + E_{\frac{1}{2}}^M \quad (\text{B1})$$

$$E_{\frac{3}{2}}^{1a} \mapsto E_{\frac{3}{2}}^{\Gamma} + E_{\frac{3}{2}}^M \quad (\text{B2})$$

$$E_{\frac{1}{2}}^{1b} \mapsto E_{\frac{1}{2}}^{\Gamma} + E_{\frac{3}{2}}^M \quad (\text{B3})$$

$$E_{\frac{3}{2}}^{1b} \mapsto E_{\frac{3}{2}}^{\Gamma} + E_{\frac{1}{2}}^M \quad (\text{B4})$$

$$E_{\frac{1}{2}}^{2c} \mapsto E_{\frac{1}{2}}^{\Gamma} + E_{\frac{3}{2}}^{\Gamma} + E_{\frac{1}{2}}^M + E_{\frac{3}{2}}^M \quad (\text{B5})$$

$$E_{\frac{1}{2}}^{4d} \mapsto 2E_{\frac{1}{2}}^{\Gamma} + 2E_{\frac{3}{2}}^{\Gamma} + 2E_{\frac{1}{2}}^M + 2E_{\frac{3}{2}}^M \quad (\text{B6})$$

Here we use the symbol of an irreducible rep (irrep) decorated with a wyckoff position to represent the WFs forming this irrep at this wyckoff position, and use the symbol of an irrep decorated with a momentum to represent the bands forming this irrep at this momentum. In the following, we will make use of these mappings.

1. Gauge invariant Wannier centers at $1a$ (site)

As will be proved latter, a set of WFs at $1a$ can be moved away by a symmetric gauge transformation only if they form a rep consist of an even number of combined

rep $E_{\frac{1}{2}}^{1a} + E_{\frac{3}{2}}^{1a}$. Therefore, the conclusion is that, for a given a set of WFs at $1a$, taking off all the even number of the rep $E_{\frac{1}{2}}^{1a} + E_{\frac{3}{2}}^{1a}$, the left WFs consisted of

$$n \left(E_{\frac{1}{2}}^{1a} + E_{\frac{3}{2}}^{1a} \right) + m E_{\frac{1}{2}}^{1a} + m' E_{\frac{3}{2}}^{1a} \quad (\text{B7})$$

, where $n = 0, 1$, and one of m m' equals to zero, will stay still under any symmetry allowed gauge transformation. We will prove this statement in three steps.

Firstly, we will show that the eight WFs forming the rep $2E_{\frac{1}{2}}^{1a} + 2E_{\frac{3}{2}}^{1a}$ can be moved to four Kramers' pairs at $4d$ positions without breaking any symmetry. Apply an unitary transform for the bases in $2E_{\frac{1}{2}}^{1a} + 2E_{\frac{3}{2}}^{1a}$

$$\begin{aligned} |w_1\rangle &= e^{-i\frac{\pi}{4}} \left| \frac{1}{2} \right\rangle_A + e^{-i\frac{\pi}{4}} \left| \frac{1}{2} \right\rangle_B \\ &+ e^{i\frac{\pi}{4}} \left| \frac{3}{2} \right\rangle_A + e^{i\frac{\pi}{4}} \left| \frac{3}{2} \right\rangle_B \end{aligned} \quad (\text{B8})$$

$$|w_{i+1}\rangle = C_4 |w_i\rangle \quad i = 0, 1, 2 \quad (\text{B9})$$

$$|w_{i+4}\rangle = T |w_i\rangle \quad i = 0, 1, 2, 3 \quad (\text{B10})$$

, where the subscript A/B is used to distinguish the two same irreps, we find that the time-reversal rep has the standard form Ω , while the C_4 rep is identical with the $E_{\frac{1}{2}}^{4d}$ WFs

$$D(C_4) = \sigma_0 \otimes \begin{bmatrix} 0 & 0 & 0 & -1 \\ 1 & 0 & 0 & 0 \\ 0 & 1 & 0 & 0 \\ 0 & 0 & 1 & 0 \end{bmatrix} \quad (\text{B11})$$

Therefore, the WFs in $2E_{\frac{1}{2}}^{1a} + 2E_{\frac{3}{2}}^{1a}$ can be moved to $4d$ without breaking any symmetry. We denote this equivalent relation as $2E_{\frac{1}{2}}^{1a} + 2E_{\frac{3}{2}}^{1a} \sim E_{\frac{1}{2}}^{4d}$. Readers may find that such a equivalence is consistent with the BR mappings in Eq. (B1)-(B6).

Secondly, it is obvious that the left $mE_{\frac{1}{2}}^{1a}$ or $m'E_{\frac{3}{2}}^{1a}$ WFs also can not be gauged away because the BR generated from $mE_{\frac{1}{2}}^{1a}$ or $m'E_{\frac{3}{2}}^{1a}$ can not be reproduced by any combination of WFs at other sites.

Thus, to complete the proof, we only need to prove a single rep $E_{\frac{1}{2}}^{1a} + E_{\frac{3}{2}}^{1a}$ must stay at $1a$ under any symmetric gauge transformation. From the BR mappings, we find that $E_{\frac{1}{2}}^{1a} + E_{\frac{3}{2}}^{1a}$ can only be moved to $E_{\frac{1}{2}}^{1b} + E_{\frac{3}{2}}^{1b}$ or $E_{\frac{1}{2}}^{2c}$. Such transformations are very unnatural from an intuitive perspective, because if we continuously move the four WFs at $1a$ to $1b$ or $2c$, the intermediate process will break either time-reversal or C_4 . (Enforced by the C_4 symmetry, the four WFs must move to four different directions, leading to separation of Kramers' pairs). To prove this statement, here we show that the gauge transformation from $E_{\frac{1}{2}}^{1a} + E_{\frac{3}{2}}^{1a}$ to $E_{\frac{1}{2}}^{1b} + E_{\frac{3}{2}}^{1b}$ or $E_{\frac{1}{2}}^{2c}$ must be

singular. Let us first consider the transformation from $E_{\frac{1}{2}}^{1a} + E_{\frac{3}{2}}^{1a}$ to $E_{\frac{1}{2}}^{1b} + E_{\frac{3}{2}}^{1b}$. For convenience, here we choose the WF bases with a ‘‘cyclical’’ gauge

$$|w_1\rangle = e^{-i\frac{\pi}{4}} \left| \frac{1}{2} \right\rangle + e^{-i\frac{\pi}{4}} \left| \frac{\bar{1}}{2} \right\rangle + e^{i\frac{\pi}{4}} \left| \frac{3}{2} \right\rangle + e^{i\frac{\pi}{4}} \left| \frac{\bar{3}}{2} \right\rangle \quad (\text{B12})$$

$$|w_{i+1}\rangle = C'_4 |w_i\rangle \quad i = 1, 2, 3 \quad (\text{B13})$$

where C'_4 is the rotation operation centered at $1a$ and $1b$ for the $E_{\frac{1}{2}}^{1a} + E_{\frac{3}{2}}^{1a}$ and $E_{\frac{1}{2}}^{1b} + E_{\frac{3}{2}}^{1b}$ WFs, respectively. In this gauge, for both $1a$ and $1b$ positions, $|w_i\rangle$ and $|w_{i+2}\rangle$ form a Kramers’ pair and the time-reversal rep matrix has the standard form Ω . According to Eq. (A11) the C_4 sewing matrices generated from $|w_i\rangle$ at $1a$ and $1b$ positions can be derived respectively as

$$D^{\mathbf{k}} = W = \begin{bmatrix} 0 & 0 & 0 & -1 \\ 1 & 0 & 0 & 0 \\ 0 & 1 & 0 & 0 \\ 0 & 0 & 1 & 0 \end{bmatrix} \quad (\text{B14})$$

$$\tilde{D}^{\mathbf{k}} = W e^{-ik_y} \quad (\text{B15})$$

Now assume there is a well defined gauge transformation $U(\mathbf{k})$ that relates these two sets of WFs, then from Eq. (A10) and (A12) such a gauge transform must satisfy

$$U(-\mathbf{k}) = \Omega U^*(\mathbf{k}) \Omega^T \quad (\text{B16})$$

$$U(C_4\mathbf{k}) = W U(\mathbf{k}) W^\dagger e^{ik_y} \quad (\text{B17})$$

leading to the equation $U^*(\mathbf{k}) = U(\mathbf{k}) e^{ik_x + ik_y}$. Thus we can write $U(\mathbf{k})$ as an orthogonal matrix $O(\mathbf{k})$ multiplied by a phase factor

$$U(\mathbf{k}) = O(\mathbf{k}) e^{-\frac{i}{2}(k_x + k_y)} \quad O(\mathbf{k}) \in O(n) \quad (\text{B18})$$

Substitute this back to Eq. (B16) and (B17), we get the constraints on $O(\mathbf{k})$ as (i) $O(-\mathbf{k}) = \Omega O(\mathbf{k}) \Omega^T$ and (ii) $O(C_4\mathbf{k}) = W O(\mathbf{k}) W^\dagger$, wherein the first constraint is implied by the second one. By requiring $U(\mathbf{k})$ to be periodic, we get another two constraints as (iii) $O(k_x + 2\pi, k_y) = -O(\mathbf{k})$ and (iv) $O(k_x, k_y + 2\pi) = -O(\mathbf{k})$. In fact, such constraints make $O(\mathbf{k})$ must be singular at some momenta. To see this, express $O(\mathbf{k})$ as

$$O(\mathbf{k}) = \xi \cdot \exp(-i\mathfrak{H}(\mathbf{k})) \quad (\text{B19})$$

where $\xi = \pm 1$ is the determinant, and $\mathfrak{H}(\mathbf{k})$ is a 4 by 4 imaginary Hermitian matrix parameterized as

$$\begin{aligned} \mathfrak{H}(\mathbf{k}) = & \omega(\mathbf{k}) [n_1(\mathbf{k}) \tau_y \sigma_x + n_2(\mathbf{k}) \tau_0 \sigma_y + n_3(\mathbf{k}) \tau_y \sigma_z] \\ & + \theta(\mathbf{k}) [m_1(\mathbf{k}) \tau_z \sigma_y + m_2(\mathbf{k}) \tau_x \sigma_y + m_3(\mathbf{k}) \tau_y \sigma_0] \end{aligned} \quad (\text{B20})$$

Here we take the convention that ω, θ are real and positive, and $\mathbf{n} = (n_1 n_2 n_3)^T$, $\mathbf{m} = (m_1 m_2 m_3)^T$ are unit

vectors. It should be noticed that as the first three matrices and the last three matrices respectively form a set of $SU(2)$ generators, and these two sets are commutative with each other, such a parameterization realizes an isomorphic mapping from $SO(4)$ to $SU(2) \times SU(2)$. Therefore, the orthogonal matrix can be expressed as a product of two commutative matrices

$$O(\mathbf{k}) = \xi \cdot \mathcal{O}^1(\mathbf{k}) \mathcal{O}^2(\mathbf{k}) \quad (\text{B21})$$

where

$$\mathcal{O}^1 = \cos \omega - i \sin \omega (n_1 \tau_y \sigma_x + n_2 \tau_0 \sigma_y + n_3 \tau_y \sigma_z) \quad (\text{B22})$$

$$\mathcal{O}^2 = \cos \theta - i \sin \theta (m_1 \tau_y \sigma_x + m_2 \tau_0 \sigma_y + m_3 \tau_y \sigma_z) \quad (\text{B23})$$

The constraints (i) and (ii) lead to

$$\omega(C_4\mathbf{k}) = \omega(\mathbf{k}) \quad \theta(C_4\mathbf{k}) = \theta(\mathbf{k}) \quad (\text{B24})$$

$$\mathbf{n}(C_4\mathbf{k}) = [n_2, n_1, -n_3]^T(\mathbf{k}) \quad (\text{B25})$$

$$\mathbf{m}(C_4\mathbf{k}) = [-m_2, m_1, m_3]^T(\mathbf{k}) \quad (\text{B26})$$

And the anti-periodic property in constraints (iii) and (iv) must be realized by either \mathcal{O}^1 or \mathcal{O}^2 . In fact, whatever which \mathcal{O} is chosen to be anti-periodic, the anti-periodic condition together with the symmetry constraints (Eq. (B24)-(B26)) will make \mathcal{O} singular at some momenta. Here we only take \mathcal{O}^1 as an example. With the anti-periodic condition, only two branches of solutions exist, the first is

$$\omega(k_x + 2\pi, k_y) = \omega(k_x, k_y + 2\pi) = \omega(\mathbf{k}) + \pi \quad (\text{B27})$$

$$\mathbf{n}(k_x + 2\pi, k_y) = \mathbf{n}(k_x, k_y + 2\pi) = \mathbf{n}(\mathbf{k}) \quad (\text{B28})$$

and the second is

$$\omega(\mathbf{k}) = \frac{\pi}{2} \quad (\text{B29})$$

$$\mathbf{n}(k_x + 2\pi, k_y) = \mathbf{n}(k_x, k_y + 2\pi) = -\mathbf{n}(\mathbf{k}) \quad (\text{B30})$$

Obviously, the first breaks the C_4 symmetry constraint (Eq. (B24)) because $\omega(\pi, 0) = \omega(-\pi, 0) + \pi$. While, the second solution is singular at $(\pi, 0)$, since there must be $\mathbf{n}(\pi, 0) = 0$ due to the C_4 constraint (Eq. (B24)) and the anti-periodic constraint (Eq. (B30)). Therefore, we achieve the conclusion that there is no smooth gauge transformation can deform $E_{\frac{1}{2}}^{1a} + E_{\frac{3}{2}}^{1a}$ to $E_{\frac{1}{2}}^{1b} + E_{\frac{3}{2}}^{1b}$. The proof for the inequivalence between $E_{\frac{1}{2}}^{1a} + E_{\frac{3}{2}}^{1a}$ and $E_{\frac{1}{2}}^{2c}$ completely parallelizes the above process.

2. Gauge invariant Wannier centers at other positions

As $1a$ and $1b$ positions can be renamed to each other by re-choosing the origin point, there is no physical difference between them and all the statements about $1a$ should also hold for $1b$. Therefore a set of WFs at $1b$ can be moved away by a symmetric gauge transformation only if the WFs consist of an even number of rep $E_{\frac{1}{2}}^{1b} + E_{\frac{3}{2}}^{1b}$. And, taking off all the even the number of the rep $E_{\frac{1}{2}}^{1b} + E_{\frac{3}{2}}^{1b}$, the centers of the left WFs are gauge invariant.

As for the $1c$ position, just like the $2E_{\frac{1}{2}}^{1a} + 2E_{\frac{3}{2}}^{1a}$ WFs in appendix B 1, a pair of $E_{\frac{1}{2}}^{2c}$ can reduce to four Kramers' pairs at the $4d$ position, i.e. $2E_{\frac{1}{2}}^{2c} \sim E_{\frac{1}{2}}^{4d}$. Thus, if there are an even number of $E_{\frac{1}{2}}^{2c}$ at the $1c$ position all of them can be gauged away to $4d$ positions, however, if there is an odd number of $E_{\frac{1}{2}}^{2c}$, at least two WFs (a Kramers' pair) will stay at $1c$ under any symmetric gauge transformation.

In summary, a set of WFs at any wyckoff position can be moved by symmetric gauge transformations if and only if the rep (of the SSG at the wyckoff position) they form is consistent with a set of $E_{\frac{1}{2}}^{4d}$ WFs. In other words, all the move of WFs should pass through $4d$ positions, which is very consistent with the intuitive picture.

3. Occupied Wannier functions for the 2D model

The occupied bands of our 2D model give the BR $E_{\frac{1}{2}}^{\Gamma} + E_{\frac{3}{2}}^{\Gamma} + E_{\frac{1}{2}}^M + E_{\frac{3}{2}}^M$, which is irrelevant with the parameter Δ since the corresponding term vanish at Γ and M . However, such a BR can not give a concrete real space information because it can be generated from $E_{\frac{1}{2}}^{1a} + E_{\frac{3}{2}}^{1a}$, or $E_{\frac{1}{2}}^{1b} + E_{\frac{3}{2}}^{1b}$, or $E_{\frac{1}{2}}^{2c}$. Here, by constructing the WFs explicitly, we will show that the occupied states are equivalent to $E_{\frac{1}{2}}^{1b} + E_{\frac{3}{2}}^{1b}$ WFs. We follow the projection procedure described in Ref. [15]. Firstly, let us guess four trial local orbitals, denoted by $|\gamma_{\alpha}\rangle$, at the home cell and define them by the model orbitals

$$|\gamma_{\alpha}\rangle = \sum_{\mathbf{R},\beta} |a_{\beta\mathbf{R}}\rangle M_{\beta\alpha}^{\mathbf{R}} \quad (\text{B31})$$

Here $|a_{\beta\mathbf{R}}\rangle$ is the β -th atomic orbital in the lattice \mathbf{R} in our 2D model, $M^{\mathbf{R}}$ (8 by 4) is the overlap matrices between atomic orbitals and the trial orbitals, and the summation $\sum_{\mathbf{R}}$ is taken only for a few lattices around the home cell. Assume $|\gamma_{\alpha}\rangle$ form the rep $E_{\frac{1}{2}}^{1b} + E_{\frac{3}{2}}^{1b}$ and limit the the summation over \mathbf{R} within $\mathbf{R}_1 = (00)$, $\mathbf{R}_2 = (10)$, $\mathbf{R}_3 = (11)$, and $\mathbf{R}_4 = (01)$, the symmetry property that $|\gamma_{\alpha}\rangle$ should satisfy can be translated to a

set of constraints on $M^{\mathbf{R}}$

$$M^{\mathbf{R}_{i+1}} = C_4 M^{\mathbf{R}_i} D^{\gamma\dagger} (C_4) \quad (\text{B32})$$

$$M^{\mathbf{R}_i} = T M^{\mathbf{R}_i} \Omega^T \quad (\text{B33})$$

Here $C_4 = \tau_z e^{-i\frac{\pi}{4}s_z}$ is the C_4 operator on the atomic orbitals, $D^{\gamma}(C_4)$ is the $E_{\frac{1}{2}}^{1b} + E_{\frac{3}{2}}^{1b}$ rep matrix of C_4 , $T = -is_y K$ is the time-reversal operator on the atomic orbitals, and Ω is the time-reversal rep on $E_{\frac{1}{2}}^{1b} + E_{\frac{3}{2}}^{1b}$. Aligning the gauge of occupied Bloch states with respect to the trial orbitals, we can define a set of projected Bloch-like states

$$|\Upsilon_{\alpha\mathbf{k}}\rangle = \sum_{n \in \text{occ}} |\psi_{n\mathbf{k}}\rangle \langle \psi_{n\mathbf{k}} | \gamma_{\alpha}\rangle \quad (\text{B34})$$

and the overlap matrix between them

$$S_{\alpha\beta}(\mathbf{k}) = \langle \Upsilon_{\alpha\mathbf{k}} | \Upsilon_{\beta\mathbf{k}}\rangle \quad (\text{B35})$$

Then by the Löwdin orthonormalization procedure, a set of orthonormal Bloch-like states are obtained

$$|\tilde{\psi}_{\alpha\mathbf{k}}\rangle = \sum_{\beta} S_{\beta\alpha}^{-\frac{1}{2}}(\mathbf{k}) |\Upsilon_{\beta\mathbf{k}}\rangle \quad (\text{B36})$$

The WFs transformed from these Bloch-like states will be well localized and satisfy the $E_{\frac{1}{2}}^{1b} + E_{\frac{3}{2}}^{1b}$ rep as long as the overlap matrix $S(\mathbf{k})$ is non-singular over the whole Brillouin zone.

In practice, we generate a random $M^{\mathbf{R}_1}$ matrix and symmetrize it due to Eq. (B32)-(B33). A non-singular $S(\mathbf{k})$ has been successfully obtained. The WCs are also confirmed by the wilson loop method and are found indeed to locate at the $1b$ position. In the wilson loop method, the center of the α -th WF is calculated by

$$x_{\alpha} = \frac{1}{2\pi} \int dk_y x_{\alpha}(k_y) \quad (\text{B37})$$

$$y_{\alpha} = \frac{1}{2\pi} \int dk_x y_{\alpha}(k_x) \quad (\text{B38})$$

$$\begin{aligned} e^{i2\pi x_{\alpha}(k_y)} &= \langle \tilde{u}_{\alpha,0,k_y} | \tilde{u}_{\alpha,(N-1)\Delta k,k_y} \rangle \cdots \\ &\times \langle \tilde{u}_{\alpha,2\Delta k,k_y} | \tilde{u}_{\alpha,\Delta k,k_y} \rangle \langle \tilde{u}_{\alpha,\Delta k,k_y} | \tilde{u}_{\alpha,0,k_y} \rangle \end{aligned} \quad (\text{B39})$$

$$\begin{aligned} e^{i2\pi y_{\alpha}(k_x)} &= \langle \tilde{u}_{\alpha,k_y,0} | \tilde{u}_{\alpha,k_x,(N-1)\Delta k} \rangle \cdots \\ &\times \langle \tilde{u}_{\alpha,k_x,2\Delta k} | \tilde{u}_{\alpha,k_x,\Delta k} \rangle \langle \tilde{u}_{\alpha,k_x,\Delta k} | \tilde{u}_{\alpha,k_x,0} \rangle \end{aligned} \quad (\text{B40})$$

where $\Delta k = \frac{2\pi}{N}$, and $|\tilde{u}_{\alpha\mathbf{k}}\rangle$ is the periodic part of the orthonormal Bloch-like state $|\tilde{\psi}_{\alpha\mathbf{k}}\rangle$.

It should be noticed that, whatever the value of Δ takes, the occupied WCs should locate at $1b$. This is simply because the Δ term can not close the band gap and the four WFs $E_{\frac{1}{2}}^{1b} + E_{\frac{3}{2}}^{1b}$ can not be moved away from $1b$ by any adiabatic process, as proved before.

Appendix C: Wannier center flow in 3D system

1. Classification of the flows

For a 3D system with both time-reversal and C_4 symmetries, we can choose a tetragonal cell with its principal axis along the z direction and apply a Fourier transformation along z . The above conclusions about the gauge invariant 2D WCs applies for the $k_z = 0, \pi$ -slices because both the time-reversal and C_4 symmetries present there. However, in general intermediate k_z -slices, the above conclusions fail because of the absence of time-reversal symmetry. Then an immediate observation follows is that a bulk state must be in some sense nontrivial if there is a mismatch between its 2D WCs in $k_z = 0$ - and $k_z = \pi$ -slices. Specifically, such a state is either a topological insulator, if continuous C_4 -preserving gauges connecting the WCs at $k_z = 0$ - and $k_z = \pi$ -slices exist in the intermediate slices, or a topological semimetal, otherwise. Here we mainly focus on the first case, wherein each k_z -slice is equivalent to a 2D atomic insulator, while the 3D system itself is inequivalent to any atomic insulator. In this case, the bulk topology is only determined by the WFs at the $k_z = 0, \pi$ -slices, because, as the sewing matrices in the intermediate slices are completely determined by the two ends (from the compatibility relation) and all the 2D atomic insulator with same sewing matrices are topologically equivalent, all the possible evolutions must be equivalent with each other. Therefore, we conclude that, for a set of given 2D WFs at the $k_z = 0$ - and $k_z = \pi$ -slices, a nontrivial flow exists if (i) the WCs at $k_z = 0$ - and $k_z = \pi$ -slices are inequivalent with each other and (ii) the WCs at the two ends can be continuously deformed to each other by a time-reversal breaking process. Considering that the gauge invariant WCs at $k_z = 0, \pi$ -slices can only locate at $1a, 1b$ and $2c$ positions and the flows between $1a$ and $2c$ can be generated from the flows between $1b$ and $2c$ and the flows between $1b$ and $1a$, to figure out the flow classification we only need to discuss the latter two cases.

Let us start with the flows between $1b$ and $1a$. For both $1b$ and $1a$ in $k_z = 0$ - or $k_z = \pi$ -slices, we only need to study the left immovable irreps

$$n \left(E_{\frac{1}{2}} + E_{\frac{3}{2}} \right) + m E_{\frac{1}{2}} + m' E_{\frac{3}{2}} \quad (C1)$$

as discussed in appendix B1. Here $n = 0, 1$ and the one of m, m' equals to zero. Firstly, we will show that the $2m$ ($2m'$) 2D WFs in the $E_{\frac{1}{2}}$ ($E_{\frac{3}{2}}$) irreps at $1a$ or $1b$ can not move along the flow. This can be seen by presuming an infinite small move and comparing the C_4 rep matrix before and after the move. Here we take $m E_{\frac{1}{2}}^{1a}$ irreps for an example. Before the move, the C_4 rep matrix is a direct sum of $m E_{\frac{1}{2}}$ rep matrices, thus the trace gives $\text{Tr}[D(C_4)] = m\sqrt{2}$. While, after the move, the WFs locating at $4d$ positions must form a traceless $D(C_4)$, because the four equivalent $4d$ positions trans-

form to each other in turn under the C_4 rotation. Therefore the presumption of the infinite small move is untenable. Secondly, notice that a single rep $E_{\frac{1}{2}} + E_{\frac{3}{2}}$ can be separated into four WFs at $4d$ positions by a time-reversal breaking process. This can be achieved in two steps. In the first step, we take the ‘‘cyclical’’ gauge defined in Eq. (B12)-(B13), where C_4 transforms the WFs to each other in turn and time-reversal transforms $|w_i\rangle$ to $|w_{i+2}\rangle$. In the second step, we split $|w_1\rangle$ and $|w_3\rangle$ in the x direction and split the $|w_2\rangle$ and $|w_4\rangle$ in the y direction. Thus, through the $4d$ positions, there can be a flow $E_{\frac{1}{2}}^{1b} + E_{\frac{3}{2}}^{1b} \rightarrow E_{\frac{1}{2}}^{1a} + E_{\frac{3}{2}}^{1a}$ or $E_{\frac{1}{2}}^{1a} + E_{\frac{3}{2}}^{1a} \rightarrow E_{\frac{1}{2}}^{1b} + E_{\frac{3}{2}}^{1b}$, where the arrow represents a flow from $k_z = 0$ to $k_z = \pi$. Such flows are gauge invariant because both $E_{\frac{1}{2}}^{1b} + E_{\frac{3}{2}}^{1b}$ and $E_{\frac{1}{2}}^{1a} + E_{\frac{3}{2}}^{1a}$ at the two ends can not be gauged away. However, double of the flows must be trivial because the $2E_{\frac{1}{2}}^{1a} + 2E_{\frac{3}{2}}^{1a}$ or the $2E_{\frac{1}{2}}^{1b} + 2E_{\frac{3}{2}}^{1b}$ can be gauged away, as discussed in appendix B1. It should also be noticed that the flow $E_{\frac{1}{2}}^{1a} + E_{\frac{3}{2}}^{1a} \rightarrow E_{\frac{1}{2}}^{1b} + E_{\frac{3}{2}}^{1b}$ is equal to the flow $E_{\frac{1}{2}}^{1b} + E_{\frac{3}{2}}^{1b} \rightarrow E_{\frac{1}{2}}^{1a} + E_{\frac{3}{2}}^{1a}$ module a trivial flow $2E_{\frac{1}{2}}^{1a} + 2E_{\frac{3}{2}}^{1a} \rightarrow 2E_{\frac{1}{2}}^{1b} + 2E_{\frac{3}{2}}^{1b}$. Therefore, in summary, we obtain a \mathbb{Z}_2 class of the flow between $1b$ and $1a$, wherein the nontrivial element $E_{\frac{1}{2}}^{1b} + E_{\frac{3}{2}}^{1b} \rightarrow E_{\frac{1}{2}}^{1a} + E_{\frac{3}{2}}^{1a}$ manifests itself by 1D helical modes, as discussed in the text.

The discussion of the flow between $1b$ and $2c$ is much more simple. As discussed above, at $1b$ position, a nontrivial flow must start or end with $E_{\frac{1}{2}}^{1b} + E_{\frac{3}{2}}^{1b}$ irreps. While, at the side of $2c$, the flow can only merge to the $E_{\frac{1}{2}}^{2c}$ irrep because there is only such one kind of irrep at $2c$. As the C_4 sewing matrix of $E_{\frac{1}{2}}^{2c}$ irrep is consistent with the C_4 sewing matrix of $E_{\frac{1}{2}}^{4d}$, the flow $E_{\frac{1}{2}}^{1b} + E_{\frac{3}{2}}^{1b} \rightarrow E_{\frac{1}{2}}^{2c}$ indeed can be realized by a time-reversal breaking process. Similar with the $1b \rightarrow 1a$ flow, this flow also generates a \mathbb{Z}_2 class, because the double of it $2E_{\frac{1}{2}}^{1b} + 2E_{\frac{3}{2}}^{1b} \rightarrow 2E_{\frac{1}{2}}^{2c}$ can be trivialized by deformations at the two ends. What kind of surface state is manifested in this class of flow? By an isomorphic mapping from the flow to the surface dispersion, we find even number Dirac points on both the zx and the yz surfaces, indicating the bulk is a weak topological insulator.

Beware that, the two flows defined above do not give a complete classification of the time-reversal and C_4 protected 3D topological crystalline insulators, instead, they only classify the a special kind of insulators where each k_z -slice is equivalent with a 2D atomic insulator.

2. Construct the flow of the 3D model

To verify our theory, in this section we explicitly show the $1b \rightarrow 1a$ flow in our 3D model by constructing 2D WFs continuously from $k_z = 0$ - to $k_z = \pi$ -slices. As described in appendix B3, the overlap matrix in real space ($M^{\mathbf{R}}$) can be thought as the input of the construction

Appendix D: Low energy theory

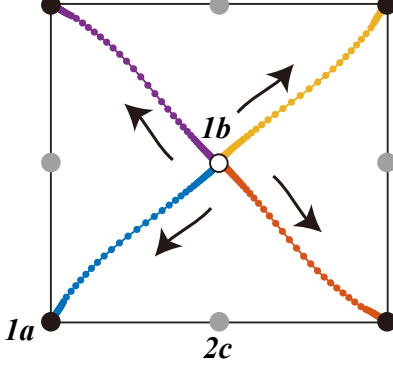


FIG. 4. The numerically calculated WC flow from $k_z = 0$ - to $k_z = \pi$ -slices in the 3D model, where the parameter Δ is set to 0.2.

procedure. Therefore, to get continuous WF gauges from $k_z = 0$ to $k_z = \pi$, we can firstly work out the overlap matrices at the two ends, i.e. $M^{\mathbf{R}}(0)$ and $M^{\mathbf{R}}(\pi)$, and then interpolate $M^{\mathbf{R}}(k_z)$ in the intermediate slices. As the $k_z = 0$ -slice is equivalent with our 2D model, we can directly use the 2D WFs constructed in appendix B 3. While, to be consistent with the flow process, here we choose the “cyclical” gauge defined in Eq. (B12)-(B13), for which the overlap matrices build for $E_{\frac{1}{2}}^{1b} + E_{\frac{3}{2}}^{1b}$ in appendix B 3, denoted as $\tilde{M}^{\mathbf{R}}$ here, should be multiplied by an unitary matrix

$$M^{\mathbf{R}_i}(0) = \tilde{M}^{\mathbf{R}_i} V^\dagger \quad (\text{C2})$$

where V can be read from the “cyclical” gauge definition in Eq. (B12)-(B13). The overlap matrix at $k_z = \pi$ can also be constructed in a similar way: randomly generate an overlap matrix and then symmetrize it. To be consistent with the flow, in $k_z = \pi$ -slice we also choose the “cyclical” gauge for the four $E_{\frac{1}{2}}^{1a} + E_{\frac{3}{2}}^{1a}$ trial orbitals and put them in the lattices $\mathbf{R}^1 = (00)$, $\mathbf{R}^2 = (10)$, $\mathbf{R}^3 = (11)$, and $\mathbf{R}^4 = (01)$, respectively. We also generate an additional $\delta M^{\mathbf{R}_i}$ term to cover the time-reversal breaking process in the intermediate slices. At last, the overlap matrix can be interpolated as

$$M^{\mathbf{R}_i}(k_z) = \left(1 - \frac{k_z}{\pi}\right) M^{\mathbf{R}_i}(0) + \frac{k_z}{\pi} M^{\mathbf{R}_i}(\pi) + \lambda \frac{k_z}{\pi} \left(1 - \frac{k_z}{\pi}\right) \delta M^{\mathbf{R}_i} \quad (\text{C3})$$

Here λ is an adjustable parameter. Within the continuous symmetric WF gauges from $k_z = 0$ to $k_z = \pi$, we calculate the evolution of WCs by the wilson loop method and plotted it in Fig. (4), which indeed coincides with the nontrivial \mathbb{Z}_2 -flow.

Another perspective to understand the 1D helical modes is from the effective low energy theory on the surfaces. As the 3D model can be thought as two copies of topological insulators plus a mixing term, on surfaces there should be two Dirac points and a mass term between them

$$H = k_1 \tau_0 \tilde{s}_1 + k_2 \tau_0 \tilde{s}_2 + m \tau_y \tilde{s}_3 \quad (\text{D1})$$

Here k_1, k_2 are the surface momenta, \tilde{s}_i are pauli matrices representing the pseudo spin. In the geometry in Fig. (2), we set $k_1 = k_y, k_2 = k_z$ for the yz surface, and $k_1 = -k_x, k_2 = k_z$ for the zx surface. For a general surface deviating from the yz plane by an angle θ , we set

$$k_1 = -\sin \theta k_x + \cos \theta k_y \quad (\text{D2})$$

$$k_2 = k_z \quad (\text{D3})$$

Then, by the symmetry analysis in the following, we show that the mass term flips its sign under the C_4 rotation, i.e. $m(\theta) = -m(\theta + \frac{\pi}{2})$. Thus, enforced by the C_4 symmetry, there must be domain walls of masses, where the helical states live, on the surfaces. Two interesting observations immediately follow. The first is that, as the domain walls are enforced by the C_4 symmetry, in general, they does not necessarily locate at the hinges. Instead, it can be anywhere on the surfaces. For our 3D model, the helical modes are pinned at the hinges by the accidental mirror symmetry. The second observation is that, the 1D helical modes are stable against to any time-reversal preserving perturbations—even the C_4 breaking perturbations—because to gap out the helical modes one need to move two domain walls separated far away in real space together to annihilate them in pair, which can not be realized by a perturbation.

Now let us derive the effective theory in Eq. (D1) and prove the mass flipping under C_4 . Firstly, we write the bulk Hamiltonian in the surface coordinates $(k_1 k_2 k_3)$, where $k_3 = \cos \theta k_x + \sin \theta k_y$, and expand it to first order of k_1, k_2 and second order of k_3

$$H = \left(-1 + \frac{k_3^2}{2}\right) \tau_0 \sigma_z s_0 + k_3 \tau_0 \sigma_x (s_x \cos \theta + s_y \sin \theta) + k_1 \tau_0 \sigma_x (-s_x \sin \theta + s_y \cos \theta) + k_2 \tau_0 \sigma_x s_z + \frac{\Delta(\theta)}{2} k_3^2 \tau_y \sigma_y s_0 \quad (\text{D4})$$

where

$$\Delta(\theta) = \Delta(\sin^2 \theta - \cos^2 \theta) \quad (\text{D5})$$

It should be noticed that, even this is a low energy theory, the property $\Delta(\theta + \frac{\pi}{2}) = -\Delta(\theta)$ holds to any order because this is enforced by the symmetry relation $C_4 \tau_y \tau_y s_0 C_4^{-1} = -\tau_y \tau_y s_0$. By the gauge transformation

$s_x \cos \theta + s_y \sin \theta \rightarrow s_3$, $-s_x \sin \theta + s_y \cos \theta \rightarrow s_1$, $s_z \rightarrow s_2$, and the replacement $k_3 \rightarrow -i\partial_3$, we get the Hamiltonian on the surface as

$$H = \left(-1 - \frac{\partial_3^2}{2}\right) \tau_0 \sigma_z s_0 - i\partial_3 \tau_0 \sigma_x s_3 - \frac{\Delta(\theta)}{2} \partial_3^2 \tau_y \sigma_y s_0 + k_1 \tau_0 \sigma_x s_1 + k_2 \tau_0 \sigma_x s_2 \quad (\text{D6})$$

Then, neglecting the k_1 , k_2 , and Δ terms, we get the zero modes equation in the $x_3 \geq 0$ semi-infinite system

$$\left[\left(1 + \frac{1}{2} \partial_x^2\right) - \tau_0 \sigma_y s_3 \partial_3\right] \psi(x_3) = 0 \quad (\text{D7})$$

with the boundary condition

$$\psi(0) = \psi(\infty) = 0 \quad (\text{D8})$$

It has four solutions

$$\psi_{\mu n}(x_3) = u_{\mu n} \frac{1}{\sqrt{\mathcal{C}}} (e^{-\lambda_+ x_3} - e^{-\lambda_- x_3}) \quad (\text{D9})$$

, where

$$\lambda_{\pm} = 1 \pm i \quad (\text{D10})$$

$$u = \frac{1}{\sqrt{2}} \begin{bmatrix} i & 0 & 0 & 0 \\ 0 & i & 0 & 0 \\ 1 & 0 & 0 & 0 \\ 0 & -1 & 0 & 0 \\ 0 & 0 & i & 0 \\ 0 & 0 & 0 & i \\ 0 & 0 & 1 & 0 \\ 0 & 0 & 0 & -1 \end{bmatrix} \quad (\text{D11})$$

Then expand the remaining terms in Eq. (D6) on these solutions, we get the effective theory

$$\mathcal{H} = k_1 \tau_0 \tilde{s}_1 + k_2 \tau_0 \tilde{s}_2 + m(\theta) \tau_y \tilde{s}_3 \quad (\text{D12})$$

where $m(\theta)$ is the mass induced by the mixing term $\Delta(\theta)$

$$m(\theta) = \frac{\Delta(\theta)}{2\mathcal{C}} \int dx_3 (e^{-\lambda_+ x_3} - e^{-\lambda_- x_3})^* \times \partial_3^2 (e^{-\lambda_+ x_3} - e^{-\lambda_- x_3}) \quad (\text{D13})$$

Therefore, as $\Delta(\theta + \frac{\pi}{2}) = -\Delta(\theta)$, the sign of mass must flip under the C_4 rotation.

Appendix E: Symmetry indicators

The \mathbb{Z}_2 -flow has provided a good physical picture and serves as a topological invariant characterizing the non-trivial states. However, for real materials, it is practically impossible to find smooth and symmetric gauges to calculate the flow. Thus it would be very useful if there is some Fu-Kane-like criterion that can diagnose the topology from merely symmetry eigenvalues. As will be shown

latter, such a criterion indeed exists if the system has an additional inversion symmetry.

We follow the newly developed symmetry indicator method^{16,17} to diagnose the topology. In this method, a BR is represented by a column vector of integers, where each entry gives the appeared number of a particular irrep at a particular high-symmetry momentum. All the admissible BRs that satisfy the compatibility relations form a linear space. While, the bases of the linear space can also be generated from a set of independent atomic BRs. Consequently, any BR can be expanded by the atomic BR bases with integer or rational fraction coefficients, wherein fraction coefficients imply some kind of nontrivial topological state.

1. Symmetry indicators in space group $P4/m$

The smallest space group containing both C_4 and inversion is $P4/m$, whose symmetry indicators form a group $\mathbb{Z}_2 \times \mathbb{Z}_4 \times \mathbb{Z}_8$. In this section, we will work out the generators of the group.

In table II, we list all the wyckoff positions and high-symmetry momenta, and the irreps of their SSGs in space group $P4/m$. By definition, a BR should be given by the numbers of irreps at Γ , M , X , Z , A , R , Λ , V , W , D , E . However, as the latter five momenta can be continuously connected to the former six momenta which have higher symmetries, the irreps at these five momenta can be inferred directly from the knowledge of the irreps at the former six momenta and the compatibility relation. Thus we conclude that the BR is completely determined by the irreps at Γ , M , X , Z , A , and R . By applying Eq. (A11) repeatedly, we have found all the independent atomic BR bases and summarize them in table III.

Now let us find out all the the compatibility relations allowed BRs. The compatibility relations consist of five constraints on the occupation number

$$\begin{aligned} & n(E_{\frac{1}{2}g}^{\Gamma}) + n(E_{\frac{3}{2}g}^{\Gamma}) + n(E_{\frac{1}{2}u}^{\Gamma}) + n(E_{\frac{3}{2}u}^{\Gamma}) \\ &= n(E_{\frac{1}{2}g}^M) + n(E_{\frac{3}{2}g}^M) + n(E_{\frac{1}{2}u}^M) + n(E_{\frac{3}{2}u}^M) \\ &= n(E_{\frac{1}{2}g}^Z) + n(E_{\frac{3}{2}g}^Z) + n(E_{\frac{1}{2}u}^Z) + n(E_{\frac{3}{2}u}^Z) \\ &= n(E_{\frac{1}{2}g}^A) + n(E_{\frac{3}{2}g}^A) + n(E_{\frac{1}{2}u}^A) + n(E_{\frac{3}{2}u}^A) \\ &= n(E_{\frac{1}{2}g}^X) + n(E_{\frac{1}{2}u}^X) \\ &= n(E_{\frac{1}{2}g}^R) + n(E_{\frac{1}{2}u}^R) \end{aligned} \quad (\text{E1})$$

and two constraints on the angular momentum conservation along ΓZ and MA

$$n(E_{\frac{1}{2}g}^{\Gamma}) + n(E_{\frac{1}{2}u}^{\Gamma}) = n(E_{\frac{1}{2}g}^Z) + n(E_{\frac{1}{2}u}^Z) \quad (\text{E2})$$

$$n(E_{\frac{1}{2}g}^M) + n(E_{\frac{1}{2}u}^M) = n(E_{\frac{1}{2}g}^A) + n(E_{\frac{1}{2}u}^A) \quad (\text{E3})$$

Site sym.	Wyckoff position		High sym. K	
	W	Irrep	K	Irrep
C_{4h}	$1a$ (000)	$E_{\frac{3}{2}u}, E_{\frac{3}{2}g}, E_{\frac{1}{2}u}, E_{\frac{1}{2}g}$	Γ (000)	$E_{\frac{3}{2}u}, E_{\frac{3}{2}g}, E_{\frac{1}{2}u}, E_{\frac{1}{2}g}$
	$1b$ ($00\frac{1}{2}$)		Z (00π)	
	$1c$ ($\frac{1}{2}\frac{1}{2}0$)		M ($\pi\pi0$)	
	$1d$ ($\frac{1}{2}\frac{1}{2}\frac{1}{2}$)		A ($\pi\pi\pi$)	
C_{2h}	$2e$ ($\frac{1}{2}00$)	$E_{\frac{1}{2}u}, E_{\frac{1}{2}g}$	X ($0\pi0$)	$E_{\frac{1}{2}u}, E_{\frac{1}{2}g}$
	$2f$ ($\frac{1}{2}0\frac{1}{2}$)		R ($0\pi\pi$)	
C_4	$2g$ (00z)	$E_{\frac{3}{2}}, E_{\frac{1}{2}}$	Λ (00u)	$E_{\frac{3}{2}}, E_{\frac{1}{2}}$
	$2h$ ($\frac{1}{2}\frac{1}{2}z$)		V ($\pi\pi u$)	
C_2	$4i$ ($\frac{1}{2}0z$)	$E_{\frac{1}{2}}$	W ($0\pi u$)	$E_{\frac{1}{2}}$
C_s	$4j$ ($xy0$)	$E_{\frac{1}{2}}$	D ($uv0$)	$E_{\frac{1}{2}}$
	$4k$ ($xy\frac{1}{2}$)		E ($uv\pi$)	
C_1	$8l$ (xyz)	$E_{\frac{1}{2}}$	GP	$E_{\frac{1}{2}}$

TABLE II. Wyckoff positions, high-symmetry momenta, and the irreps of their SSGs in space group $P4/m$ (with time-reversal symmetry).

BR		
\mathbf{A}_1	$E_{\frac{1}{2}g}^{1a}$	$E_{\frac{1}{2}g}^{\Gamma} + E_{\frac{1}{2}g}^M + E_{\frac{1}{2}g}^X + E_{\frac{1}{2}g}^Z + E_{\frac{1}{2}g}^A + E_{\frac{1}{2}g}^R$
\mathbf{A}_2	$E_{\frac{3}{2}g}^{1a}$	$E_{\frac{3}{2}g}^{\Gamma} + E_{\frac{3}{2}g}^M + E_{\frac{3}{2}g}^X + E_{\frac{3}{2}g}^Z + E_{\frac{3}{2}g}^A + E_{\frac{3}{2}g}^R$
\mathbf{A}_3	$E_{\frac{1}{2}u}^{1a}$	$E_{\frac{1}{2}u}^{\Gamma} + E_{\frac{1}{2}u}^M + E_{\frac{1}{2}u}^X + E_{\frac{1}{2}u}^Z + E_{\frac{1}{2}u}^A + E_{\frac{1}{2}u}^R$
\mathbf{A}_4	$E_{\frac{3}{2}u}^{1a}$	$E_{\frac{3}{2}u}^{\Gamma} + E_{\frac{3}{2}u}^M + E_{\frac{3}{2}u}^X + E_{\frac{3}{2}u}^Z + E_{\frac{3}{2}u}^A + E_{\frac{3}{2}u}^R$
\mathbf{A}_5	$E_{\frac{1}{2}g}^{1b}$	$E_{\frac{1}{2}g}^{\Gamma} + E_{\frac{1}{2}g}^M + E_{\frac{1}{2}g}^X + E_{\frac{1}{2}g}^Z + E_{\frac{1}{2}g}^A + E_{\frac{1}{2}g}^R$
\mathbf{A}_6	$E_{\frac{3}{2}g}^{1b}$	$E_{\frac{3}{2}g}^{\Gamma} + E_{\frac{3}{2}g}^M + E_{\frac{3}{2}g}^X + E_{\frac{3}{2}g}^Z + E_{\frac{3}{2}g}^A + E_{\frac{3}{2}g}^R$
\mathbf{A}_7	$E_{\frac{1}{2}g}^{1c}$	$E_{\frac{1}{2}g}^{\Gamma} + E_{\frac{1}{2}g}^M + E_{\frac{1}{2}g}^X + E_{\frac{1}{2}g}^Z + E_{\frac{1}{2}g}^A + E_{\frac{1}{2}g}^R$
\mathbf{A}_8	$E_{\frac{3}{2}g}^{1c}$	$E_{\frac{3}{2}g}^{\Gamma} + E_{\frac{3}{2}g}^M + E_{\frac{3}{2}g}^X + E_{\frac{3}{2}g}^Z + E_{\frac{3}{2}g}^A + E_{\frac{3}{2}g}^R$
\mathbf{A}_9	$E_{\frac{1}{2}u}^{1c}$	$E_{\frac{1}{2}u}^{\Gamma} + E_{\frac{1}{2}u}^M + E_{\frac{1}{2}u}^X + E_{\frac{1}{2}u}^Z + E_{\frac{1}{2}u}^A + E_{\frac{1}{2}u}^R$
\mathbf{A}_{10}	$E_{\frac{1}{2}g}^{1d}$	$E_{\frac{1}{2}g}^{\Gamma} + E_{\frac{1}{2}g}^M + E_{\frac{1}{2}g}^X + E_{\frac{1}{2}g}^Z + E_{\frac{1}{2}g}^A + E_{\frac{1}{2}g}^R$
\mathbf{A}_{11}	$E_{\frac{3}{2}g}^{1d}$	$E_{\frac{3}{2}g}^{\Gamma} + E_{\frac{3}{2}g}^M + E_{\frac{3}{2}g}^X + E_{\frac{3}{2}g}^Z + E_{\frac{3}{2}g}^A + E_{\frac{3}{2}g}^R$
\mathbf{A}_{12}	$E_{\frac{1}{2}g}^{2e}$	$E_{\frac{1}{2}g}^{\Gamma} + E_{\frac{1}{2}g}^{\Gamma} + E_{\frac{1}{2}g}^M + E_{\frac{1}{2}g}^M + E_{\frac{1}{2}g}^X + E_{\frac{1}{2}g}^X + E_{\frac{1}{2}g}^Z + E_{\frac{1}{2}g}^Z + E_{\frac{1}{2}g}^A + E_{\frac{1}{2}g}^A + E_{\frac{1}{2}g}^R + E_{\frac{1}{2}g}^R$
\mathbf{A}_{13}	$E_{\frac{1}{2}g}^{2f}$	$E_{\frac{1}{2}g}^{\Gamma} + E_{\frac{1}{2}g}^{\Gamma} + E_{\frac{1}{2}g}^M + E_{\frac{1}{2}g}^M + E_{\frac{1}{2}g}^X + E_{\frac{1}{2}g}^X + E_{\frac{1}{2}g}^Z + E_{\frac{1}{2}g}^Z + E_{\frac{1}{2}g}^A + E_{\frac{1}{2}g}^A + E_{\frac{1}{2}g}^R + E_{\frac{1}{2}g}^R$

TABLE III. Atomic BR bases of space group $P4/m$. In the first, second, and third columns, we list the notations of atomic BR bases, the irreps in real space to generate it, and the BR in momentum space, respectively.

Solve these linear equations, we get 13 independent BR generators, wherein 10 of them are atomic BRs, while the other 3 are not. The three nontrivial generators can be chosen as

$$\mathbf{B}_{\mathbb{Z}_2} = E_{\frac{1}{2}g}^{\Gamma} + E_{\frac{1}{2}g}^M + E_{\frac{1}{2}g}^X + E_{\frac{1}{2}g}^Z + E_{\frac{1}{2}g}^A + E_{\frac{1}{2}g}^R \quad (\text{E4})$$

$$\mathbf{B}_{\mathbb{Z}_4} = E_{\frac{1}{2}u}^{\Gamma} + E_{\frac{1}{2}g}^M + E_{\frac{1}{2}g}^X + E_{\frac{1}{2}u}^Z + E_{\frac{1}{2}g}^A + E_{\frac{1}{2}u}^R \quad (\text{E5})$$

$$\mathbf{B}_{\mathbb{Z}_8} = E_{\frac{1}{2}u}^{\Gamma} + E_{\frac{1}{2}g}^M + E_{\frac{1}{2}g}^X + E_{\frac{1}{2}g}^Z + E_{\frac{1}{2}g}^A + E_{\frac{1}{2}u}^R \quad (\text{E6})$$

Here \mathbb{Z}_N represents that $N\mathbf{B}_{\mathbb{Z}_N}$ is an atomic BR. Therefore, the BRs of $P4/m$ can be classified into $2 \times 4 \times 8$ classes, each of them is given by three integers (mnl) that define the representative BR $m\mathbf{B}_{\mathbb{Z}_2} + n\mathbf{B}_{\mathbb{Z}_4} + l\mathbf{B}_{\mathbb{Z}_8}$, with $m = 0, 1$, $n = 0, 1, 2, 3$, and $l = 0, 1 \cdots 7$.

2. Understand the indicators

From the parity criterion, we find that all these three generators correspond to weak or strong topological insulators. Specifically, $\mathbf{B}_{\mathbb{Z}_2}$ has a nontrivial weak index $\mathbb{Z}_2(110;0)$, $\mathbf{B}_{\mathbb{Z}_4}$ also has a nontrivial weak index $\mathbb{Z}_2(001;0)$, whereas $\mathbf{B}_{\mathbb{Z}_8}$ has a nontrivial strong index $\mathbb{Z}_2(111;1)$.

The double of $\mathbf{B}_{\mathbb{Z}_4}$ or $\mathbf{B}_{\mathbb{Z}_8}$ corresponds to mirror ($M_z = PC_2$) protected topological crystalline insulators, wherein $2\mathbf{B}_{\mathbb{Z}_4}$ has mirror Chern number 2 (mod 4) in both the $k_z = 0$ - and $k_z = \pi$ -slices, while $2\mathbf{B}_{\mathbb{Z}_8}$ has mirror Chern number 2 (mod 4) in the $k_z = 0$ -slice and mirror Chern number 0 (mod 4) in the $k_z = \pi$ -slice. This can be proved by firstly divide the eigenstates at $k_z = 0$ -slice ($k_z = \pi$ -slice) into two sectors according to their M_z eigenvalues and then apply the following Chern number

Fu-Kane-like formula in each sector³²

$$-i^C = \prod_{n \in \text{occ}} \xi_n(\Gamma) \xi_n(M) \zeta_n(X) \quad (\text{E7})$$

Here $\xi_n(\Gamma)$ is the C_4 eigenvalue of the n -band at Γ , $\xi_n(M)$ is the C_4 eigenvalue of the n -band at M , $\zeta_n(X)$ is the C_2 eigenvalue of the n -band at X , and C is the Chern number. Specifically, consider the $k_z = 0$ -slice in $2\mathbf{B}_{\mathbb{Z}_4}$, for the $M_z = i$ sector, we have $\xi(\Gamma) = e^{-i\frac{\pi}{4}}, e^{-i\frac{\pi}{4}}$, $\xi(M) = e^{i\frac{\pi}{4}}, e^{i\frac{\pi}{4}}$, and $\zeta(\Gamma) = i, i$, which gives the mirror Chern number 2 (mod 4). Similarly, we also have the mirror Chern number 2 (mod 4) for the $k_z = \pi$ -slice. Follow the same calculation, we find that in $2\mathbf{B}_{\mathbb{Z}_8}$, the $k_z = 0$ -slice has mirror Chern number 2 (mod 4) while the $k_z = \pi$ plane has mirror Chern number 0 (mod 4).

Now the only left generator is $4\mathbf{B}_{\mathbb{Z}_8}$. To figure out it, let us firstly generalize the mappings in Eq. (B1)-(B4) to the case with inversion symmetry. Treating $k_z = 0$ - and $k_z = \pi$ -slices as two 2D systems and applying Eq. (A11), we find that

$$E_{\frac{1}{2}g}^{1a}(0/\pi) \mapsto E_{\frac{1}{2}g}^{\Gamma/Z} + E_{\frac{1}{2}g}^{M/A} + E_{\frac{1}{2}g}^{X/R} \quad (\text{E8})$$

$$E_{\frac{3}{2}g}^{1a}(0/\pi) \mapsto E_{\frac{3}{2}g}^{\Gamma/Z} + E_{\frac{3}{2}g}^{M/A} + E_{\frac{3}{2}g}^{X/R} \quad (\text{E9})$$

$$E_{\frac{1}{2}u}^{1a}(0/\pi) \mapsto E_{\frac{1}{2}u}^{\Gamma/Z} + E_{\frac{1}{2}u}^{M/A} + E_{\frac{1}{2}u}^{X/R} \quad (\text{E10})$$

$$E_{\frac{3}{2}u}^{1a}(0/\pi) \mapsto E_{\frac{3}{2}u}^{\Gamma/Z} + E_{\frac{3}{2}u}^{M/A} + E_{\frac{3}{2}u}^{X/R} \quad (\text{E11})$$

$$E_{\frac{1}{2}g}^{1b}(0/\pi) \mapsto E_{\frac{1}{2}g}^{\Gamma/Z} + E_{\frac{3}{2}g}^{M/A} + E_{\frac{1}{2}u}^{X/R} \quad (\text{E12})$$

$$E_{\frac{3}{2}g}^{1b}(0/\pi) \mapsto E_{\frac{3}{2}g}^{\Gamma/Z} + E_{\frac{1}{2}g}^{M/A} + E_{\frac{1}{2}u}^{X/R} \quad (\text{E13})$$

$$E_{\frac{1}{2}u}^{1b}(0/\pi) \mapsto E_{\frac{1}{2}u}^{\Gamma/Z} + E_{\frac{3}{2}u}^{M/A} + E_{\frac{1}{2}g}^{X/R} \quad (\text{E14})$$

$$E_{\frac{3}{2}u}^{1b}(0/\pi) \mapsto E_{\frac{3}{2}u}^{\Gamma/Z} + E_{\frac{1}{2}u}^{M/A} + E_{\frac{1}{2}g}^{X/R} \quad (\text{E15})$$

Therefore, the $4\mathbf{B}_{\mathbb{Z}_8}$ can be interpreted as

$$E_{\frac{1}{2}g}^{1b}(0) + E_{\frac{3}{2}g}^{1b}(0) + E_{\frac{1}{2}u}^{1a}(\pi) + E_{\frac{3}{2}g}^{1a}(\pi) \mapsto 4\mathbf{B}_{\mathbb{Z}_8} \quad (\text{E16})$$

where the WCs start at the plaquette center ($k_z = 0$) and end the site ($k_z = \pi$). As all the atomic BRs can not imply any WC flow, all the BRs in the (004) class would enforce the nontrivial \mathbb{Z}_2 -flow.

3. Matlab script

Here we also provide a Matlab script to automatically calculate the symmetry indicator of a given BR of the space group $P4/m$.

```

1 clear ;
2 %
3 % bases =====
4 %
5 e_G12g=zeros(20,1); e_G12g(1)=1; e_G32g=zeros(20,1); e_G32g(2)=1;
6 e_G12u=zeros(20,1); e_G12u(3)=1; e_G32u=zeros(20,1); e_G32u(4)=1;
7
8 e_M12g=zeros(20,1); e_M12g(5)=1; e_M32g=zeros(20,1); e_M32g(6)=1;
9 e_M12u=zeros(20,1); e_M12u(7)=1; e_M32u=zeros(20,1); e_M32u(8)=1;
10
11 e_X12g=zeros(20,1); e_X12g(9)=1; e_X12u=zeros(20,1); e_X12u(10)=1;
12
13 e_Z12g=zeros(20,1); e_Z12g(11)=1; e_Z32g=zeros(20,1); e_Z32g(12)=1;
14 e_Z12u=zeros(20,1); e_Z12u(13)=1; e_Z32u=zeros(20,1); e_Z32u(14)=1;
15
16 e_A12g=zeros(20,1); e_A12g(15)=1; e_A32g=zeros(20,1); e_A32g(16)=1;
17 e_A12u=zeros(20,1); e_A12u(17)=1; e_A32u=zeros(20,1); e_A32u(18)=1;
18
19 e_R12g=zeros(20,1); e_R12g(19)=1; e_R12u=zeros(20,1); e_R12u(20)=1;
20 %
21 % AI bases =====
22 %
23 AA=[
```

```

24 e_G12g + e_M12g + e_X12g + e_Z12g + e_A12g + e_R12g, ... % 1a 1/2g
25 e_G32g + e_M32g + e_X12g + e_Z32g + e_A32g + e_R12g, ... % 1a 3/2g
26 e_G12u + e_M12u + e_X12u + e_Z12u + e_A12u + e_R12u, ... % 1a 1/2u
27 e_G32u + e_M32u + e_X12u + e_Z32u + e_A32u + e_R12u, ... % 1a 3/2u
28 e_G12g + e_M12g + e_X12g + e_Z12u + e_A12u + e_R12u, ... % 1b 1/2g
29 e_G32g + e_M32g + e_X12g + e_Z32u + e_A32u + e_R12u, ... % 1b 3/2g
30 e_G12g + e_M32g + e_X12u + e_Z12g + e_A32g + e_R12u, ... % 1c 1/2g
31 e_G32g + e_M12g + e_X12u + e_Z32g + e_A12g + e_R12u, ... % 1c 3/2g
32 e_G12u + e_M32u + e_X12g + e_Z12u + e_A32u + e_R12g, ... % 1c 1/2u
33 e_G12g + e_M32g + e_X12u + e_Z12u + e_A32u + e_R12g, ... % 1d 1/2g
34 e_G32g + e_M12g + e_X12u + e_Z32u + e_A12u + e_R12g, ... % 1d 3/2g
35 e_G12g + e_G32g + e_M12u + e_M32u + e_X12g + e_X12u ...
36 + e_Z12g + e_Z32g + e_A12u + e_A32u + e_R12g + e_R12u, ... % 2e 1/2g
37 e_G12g + e_G32g + e_M12u + e_M32u + e_X12g + e_X12u ...
38 + e_Z12u + e_Z32u + e_A12g + e_A32g + e_R12g + e_R12u % 2f 1/2g
39 ];
40 %
41 % Nontrivial generators =====
42 %
43 BZ2 = e_G12g + e_M12g + e_X12g + e_Z12g + e_A12g + e_R12u;
44 BZ4 = e_G12u + e_M12g + e_X12g + e_Z12u + e_A12g + e_R12g;
45 BZ8 = e_G12u + e_M12g + e_X12g + e_Z12g + e_A12g + e_R12g;
46 %
47 % diagnose the BR =====
48 %
49 BR = e_G12g + e_G32u + e_M12u + e_M32g + e_X12g + e_X12u ...
50 + e_Z12u + e_Z32g + e_A12u + e_A32g + e_R12g + e_R12u;
51 %
52 [m, n, l] = fun_class83( BR, AA, BZ2, BZ4, BZ8);
53 fprintf('m, n, l= %d, %d, %d\n',m,n,l);
54 %
55 % subroutine to calculate the indicator =====
56 %
57 function [ n1, n2, n3 ] = fun_class83( bb, AA, b1,b2,b3 )
58 tol=1e-3;
59 for n1=0:1
60     for n2=0:3
61         for n3=0:7
62             btmp = n1*b1+n2*b2+n3*b3;
63             CC=AA\(btmp - bb);
64             err = norm(CC-round(CC));
65             %
66             %fprintf('%d %d %d %f\n', n1, n2, n3, err)
67             %
68             if err < tol
69                 break;
70             end
71         end
72         %
73         if err < tol
74             break;
75         end
76     end
77     %
78     if err < tol
79         break;
80     end
81 end

```

```

82
83 if err>=tol
84     n1=-1;
85     n2=-1;
86     n3=-1;
87 end
88
89 end

```

where the variable BR is the input band representation, and (mnl) is the indicator calculated from BR. For practical application, one only need to replace the definition of BR (line 49 in the code). It should be noticed that, this script is not limited to the space group $P4/m$, but is

applicable to any space group containing C_4 and inversion symmetries.

We have used our 3D model to verify the symmetry indicator, which indeed gives (004).

-
- * cfang@iphy.ac.cn
- ¹ Z.-C. Gu and X.-G. Wen, *Phys. Rev. B* **80**, 155131 (2009).
 - ² X. Chen, Z.-C. Gu, Z.-X. Liu, and X.-G. Wen, **338**, 1604 (2012).
 - ³ X. Chen, Z.-X. Liu, and X.-G. Wen, *Phys. Rev. B* **84**, 235141 (2011).
 - ⁴ F. D. M. Haldane, *Phys. Rev. Lett.* **50**, 1153 (1983).
 - ⁵ M. Z. Hasan and C. L. Kane, *Rev. Mod. Phys.* **82**, 3045 (2010).
 - ⁶ X.-L. Qi and S.-C. Zhang, *Rev. Mod. Phys.* **83**, 1057 (2011).
 - ⁷ L. Fu, *Phys. Rev. Lett.* **106**, 106802 (2011).
 - ⁸ A. M. Turner, Y. Zhang, and A. Vishwanath, *Phys. Rev. B* **82**, 241102 (2010).
 - ⁹ T. L. Hughes, E. Prodan, and B. A. Bernevig, *Phys. Rev. B* **83**, 245132 (2011).
 - ¹⁰ T. H. Hsieh, H. Lin, J. Liu, W. Duan, A. Bansil, and L. Fu, **3**, 982 EP (2012).
 - ¹¹ W. A. Benalcazar, B. A. Bernevig, and T. L. Hughes, [10.1126/science.aah6442](https://arxiv.org/abs/10.1126/science.aah6442).
 - ¹² F. Schindler, A. Cook, M. G. Vergniory, and T. Neupert, in *APS March Meeting* (2017).
 - ¹³ L. Fu, C. L. Kane, and E. J. Mele, *Phys. Rev. Lett.* **98**, 106803 (2007).
 - ¹⁴ N. Marzari and D. Vanderbilt, *Phys. Rev. B* **56**, 12847 (1997).
 - ¹⁵ A. A. Soluyanov and D. Vanderbilt, *Phys. Rev. B* **83**, 035108 (2011).
 - ¹⁶ H. C. Po, A. Vishwanath, and H. Watanabe, *Nature Communications* **8**, 50 (2017).
 - ¹⁷ B. Bradlyn, L. Elcoro, J. Cano, M. G. Vergniory, Z. Wang, C. Felser, M. I. Aroyo, and B. A. Bernevig, *Nature* **547**, 298 (2017).
 - ¹⁸ J. C. Y. Teo and C. L. Kane, *Phys. Rev. B* **89**, 085101 (2014).
 - ¹⁹ Y. Oreg, E. Sela, and A. Stern, *Phys. Rev. B* **89**, 115402 (2014).
 - ²⁰ T. Neupert, C. Chamon, C. Mudry, and R. Thomale, *Phys. Rev. B* **90**, 205101 (2014).
 - ²¹ R. Thorngren and D. V. Else, [arXiv:1612.00846](https://arxiv.org/abs/1612.00846) (2016).
 - ²² S.-J. Huang, H. Song, Y.-P. Huang, and M. Hermele, [arXiv:1705.09243](https://arxiv.org/abs/1705.09243) (2017).
 - ²³ C. Wang and M. Cheng, in preparation (2017).
 - ²⁴ I. Affleck, T. Kennedy, E. H. Lieb, and H. Tasaki, *Phys. Rev. Lett.* **59**, 799 (1987).
 - ²⁵ I. Affleck, T. Kennedy, E. H. Lieb, and H. Tasaki, *Communications in Mathematical Physics* **115**, 477 (1988).
 - ²⁶ M. Levin and Z.-C. Gu, *Phys. Rev. B* **86**, 115109 (2012).
 - ²⁷ R. Resta, *Ferroelectrics* **136**, 51 (1992).
 - ²⁸ R. D. King-Smith and D. Vanderbilt, *Physical Review B* **47**, 1651 (1993).
 - ²⁹ R. Yu, X. L. Qi, A. Bernevig, Z. Fang, and X. Dai, *Phys. Rev. B* **84**, 075119 (2011).
 - ³⁰ L. Fidkowski, T. S. Jackson, and I. Klich, *Phys. Rev. Lett.* **107**, 036601 (2011).
 - ³¹ S. L. Altmann and P. Herzig, *Point-group theory tables* (Clarendon Press, 1994).
 - ³² C. Fang, M. J. Gilbert, and B. A. Bernevig, *Phys. Rev. B* **86**, 115112 (2012).